J Mater Sci: Mater Med (2010) 21:2711–2722
DOI 10.1007/s10856-010-4115-4

Hydroxyapatite formation from cuttlefish bones: kinetics

H. Ivankovic · E. Tkalcec · S. Orlic · G. Gallego Ferrer · Z. Schauperl

Received: 19 February 2010 / Accepted: 7 June 2010 / Published online: 22 June 2010

Abstract Highly porous hydroxyapatite ($Ca_{10}(PO_4)_6 \cdot (OH)_2$, HA) was prepared through hydrothermal transformation of aragonitic cuttlefish bones (*Sepia officinalis* L. Adriatic Sea) in the temperature range from 140 to 220°C for 20 min to 48 h. The phase composition of converted hydroxyapatite was examined by quantitative X-ray diffraction (XRD) using Rietveld structure refinement and Fourier transform infrared spectroscopy (FTIR). Johnson–Mehl–Avrami (JMA) approach was used to follow the kinetics and mechanism of transformation. Diffusion controlled one dimensional growth of HA, predominantly along the *a*-axis, could be defined. FTIR spectroscopy determined B-type substitutions of CO_3^{2-} groups. The morphology and microstructure of converted HA was examined by scanning electron microscopy. The general architecture of cuttlefish bones was preserved after hydrothermal treatment and the cuttlefish bones retained its form with the same channel size ($\sim 80 \times 300$ μm). The formation of dandelion-like HA spheres with diameter from 3 to 8 μm were observed on the surface of lamellae, which further transformed into various radially oriented nanoplates and nanorods with an average diameter of about 200–300 nm and an average length of about 8–10 μm.

H. Ivankovic (✉) · E. Tkalcec · S. Orlic
Faculty of Chemical Engineering and Technology, University of Zagreb, Zagreb, Croatia
e-mail: hivan@fkit.hr

G. Gallego Ferrer
Centro de Biomateriales, Universidad Politecnica de Valencia, Valencia, Spain

Z. Schauperl
Faculty of Mechanical Engineering and Naval Architecture, University of Zagreb, Zagreb, Croatia

1 Introduction

Hydroxyapatite (HA) is being extensively used for bio implantation [1, 2]. Due to similarity in the mineral constituents with natural hard tissues (bones and teeth) it has excellent biocompatibility and osteoconductivity [2]. However, due to its low mechanical strength its usage is restricted on phase reinforcement in composites, coating on metal implants, granular fills for direct incorporation into human tissues and recently on production of porous scaffolds, which can host the biological activities in a physiological manner. The scaffold acts as a temporary substrate or template, providing the necessary support for the cell growth and maintenance their differentiated functions. Furthermore, its architecture defines the final shape of the new bone [3]. Thus, the success of bone tissue engineering applications depends, to a large extent on the performance of the scaffolds. In order to get three dimensional and highly interconnected macroporous network for cell growth and flow transport of nutrients and metabolic waste, scaffolds should have appropriate porosity, pore size and pore structure.

Rapid prototyping [4] or the foaming agents [5] have been employed to produce porous scaffolds of synthetic hydroxyapatite. However, the methods are expensive and not well defined concerning the internal porous architecture. Therefore the interest is addressed to development of bone-scaffolds from biogenetic aragonite ($CaCO_3$). The most of the synthetic HA is stoichiometric with chemical composition $Ca_{10}(PO_4)_6(OH)_2$. By contrast, HA prepared from natural sources, which primarily include corals, nacres, animal bones, exoskeletons, etc. is no stoichiometric, and have other ions incorporated, mainly CO_3^{2-}, trace of Na^+, Mg^{2+}, Fe^{2+}, F^-, Cl^- [6]. CO_3^{2-} containing HA has gained much attention as it can be more easily resorbed

by the living cells in comparison with stoichiometric HA, and therefore it leads to faster bone regeneration. CO_3^{2-} can be substituted for either OH^- (A-type) or PO_4^{3-} (B-type) groups in the structure of hydroxyapatite. Sometimes, both A-type and B-type substitutions can also occur [7, 8]. Several attempts to convert natural aragonite structures (e.g., corals, nacres, etc.) hydrothermally to hydroxyapatite have been reported [9–16]. The ability of fast transformation of natural aragonitic structure into HA, even at room temperature, has been reported by Ni and Ratner [11]. Rocha and coworkers [12–14] were the first who performed the transformation of aragonitic cuttlefish bones by hydrothermal treatment into HA. The inorganic part of cuttlefish bone is a lamellar mineralized porous structure of aragonite. Its highly channeled structure favors the diffusion of the reaction solution towards the aragonite and its fast transformation to HA. Hydrothermal synthesis involves the treatment of precursors at elevated temperatures and pressures. The reaction sequences in hydrothermal systems are complex and in most cases the information regarding the course of reactions is only partial. Various mechanisms of transformation of $CaCO_3$ into HA are assumed in literature. Eysel and Roy [15] proposed topotactic reaction of aragonite to HA, dissolution and precipitation reaction of aragonitic nacres to HA was proposed by Ni and Ratner [11]. Zaremba et al. [16] studying the aragonite transformation in gastropod (abalone) nacres suggested dissolution–recrystallization mechanism of the HA growth, whereas Yoshimura et al. [17], proposed dissolution-precipitation mechanism followed by nucleation and growth of HA on the surface of calcite ($CaCO_3$). According to Jinawath et al. [18], aragonite in porites was initially transformed into intermediate $CaHPO_4$ (DCPA) at pH 2–4, which at pH > 6 transformed into HA. The authors also proposed dissolution–recrystallization mechanism as driving force for hydroxyapatite growth. To the best of our knowledge, kinetic parameters (the rate constant k, the activation energy) of biogenetic aragonite transformation into hydroxyapatite are not available in literature. On the other hand, there are papers dealing with the kinetics of hydroxyapatite formation from various synthetic precursors. Huang and coworkers [19], studying the kinetics of electrochemical deposition and post-hydrothermal synthesis of HA from brushite (DCPD–$CaHPO_4{\cdot}2H_2O$), have found an Arrhenius relationship between the formation rate and temperature with an apparent activation energy of 94.4 kJ/mol. Liu et al. [20], studying the mechanism and kinetics of HA precipitation from aqueous solution at pH 10–11 found that HA formation is surface controlled process with an activation energy of 95 kJ/mol. Lopatin et al. [21], studying the crystallization kinetics of sol–gel derived hydroxyapatite thin films, have found that the activation energy depends on the pre-treatment of gels. The activation energy is higher (231 kJ/mol) in the aged compared to non-aged (189 kJ/mol) samples, indicating that the aging raises the energy barriers, thus hinders the transformation.

The aim of this work was: to study the transformation mechanism of aragonite of cuttlefish bones into HA in the dependence of temperature and time of hydrothermal treatment, and evolution of the reaction rate and activation energy using Arrhenius kinetics.

2 Materials and methods

The starting material for synthesis of hydroxyapatite was aragonitic cuttlefish bone, *Sepia officinalis* L., from the Adriatic Sea heated at 350°C for 3 h to remove the organic component of cuttlefish bone. For hydrothermal treatment pieces of about $1 \times 1 \times 2$ cm^3 cut from the internal cuttlefish bone matrix (lamellae spacing) were used, since by the pre-treatment at 350°C only the aragonite in lamellae spacing retained its structure, while aragonite from the external wall (dorsal shield) transformed into calcite. For each batch of cut cuttlefish bones the required volume of 0.6 M aqueous solution of $NH_4H_2PO_4$ was added to settle the molar ratio of Ca/P = 1.67. The obtained suspension was transferred in TEFLON lined stainless steel pressure vessel, and sealed from 140 to 220°C in the step of 20°C for various times (20 min to 48 h) in an electric furnace. The pressure inside the reactor was self-generated by water vapor. After hydrothermal treatment the reactor was cooled down and the pH of the resulting suspension was measured at RT. The converted HA was washed with boiling water and dried at 110°C for further characterization. The microstructure of heated (350°C) and hydrothermally treated (HT) cuttlefish bones has been examined by scanning electron microscopy (SEM TESCAN VEGA TS5136LS). The conversion of HT transformation was followed by X-ray diffraction analysis (Philips PW 1820 counter diffractometer with Cu Kα radiation). Changes of crystal structure and unit cell parameters of HA upon heating were followed by Rietveld structure refinement approach [22] carried out on XRD patterns collected from 15° to 120° 2θ, with steps of 0.02° and with fixed counting time of 10 s per step. The software Topas 2.1 [23] was used for the data evaluation. Holly Springs hydroxyapatite [24, 25] was used as a starting model for the refinement. For aragonite structure the model of Dickens and Bowen [26] was applied. To quantify HA transformed by hydrothermal treatment, the refinement was performed on the XRD patterns with known addition of Si. This method allowed us to follow the transformation of aragonite into HA as a function of temperature and time of hydrothermal treatment (HT). XRD patterns were also used to determine the change of crystallite size of HA along to the *c* and *a*-axes

applying the Scherrer's approximation [27] and measuring the full width at half maximum (FWHM) for (002) and (300) reflections.

Fourier transform infrared spectra (FTIR) were performed by attenuated total reflectance (ATR) spectroscopy for solids with a diamond crystal.

3 Results

3.1 Quantitative XRD powder diffraction

Figure 1 displays: (a) the schematic view of a transverse section of cuttlefish bone, (b) XRD patterns of the dorsal shield and lamellae matrix heated at 350°C for 3 h, (c) SEM micrograph of cross section of dorsal shield, and (d) SEM micrograph of the lamellae spacing of raw cuttlefish bone. The XRD patterns (Fig. 1b) show that the dorsal shield (external part) of cuttlebone was transformed into calcite by heat treatment, whereas the lamellae matrix retained the aragonitic structure. From SEM micrographs of raw cuttlefish bone the organic component between the dorsal shield and the internal matrix (Fig. 1c), as well as, around the each lamellae (Fig. 1d) of the internal spacing is well seen. Therefore, for hydrothermal (HT) treatment only pieces of internal cuttlebone matrix (lamellae spacing) were used. XRD patterns of the samples HT treated for 20 min at various temperatures are given in Fig. 2. Whereas in Table 1 the formed phases are compared with the pH values of suspensions of HT treated product. XRD analysis shows that along to still untransformed aragonite, poorly crystallized hydroxyapatite and brushite, $CaHPO_4 \cdot 2H_2O$, were determined in the samples heat treated at 140 and 160°C. The sharpness of the (020) line implies high crystallinity of brushite. With the increase of HT temperature, the amount of brushite decreases, so at 180°C just discernible amount of brushite is detected, and in the sample heated at 200°C brushite was not observed. Simultaneously the pH values of suspension increase with HT treatment from 5.34 (140°C) to 6.42 (220°C). Figure 3 displays XRD patterns of HT samples treated at various time and temperature with silicon addition as the internal

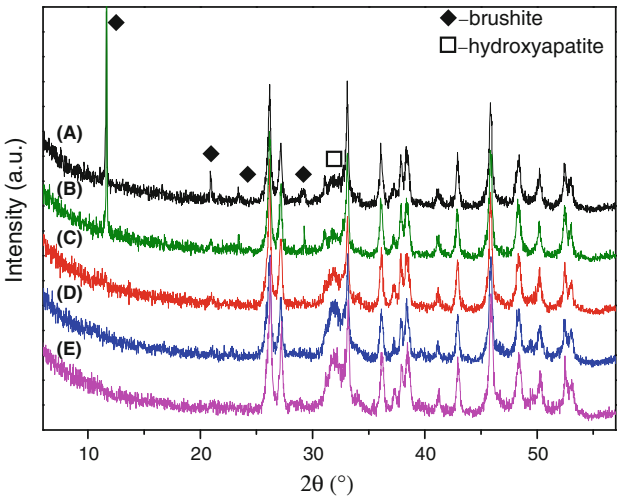

Fig. 2 XRD patterns of samples HT treated at: (*a*) 140°C, (*b*) 160°C (*c*) 180°C, (*d*) 200°C and (*e*) 220°C for 20 min. (◆) Brushite; (□) hydroxyapatite. The aragonite lines are not marked

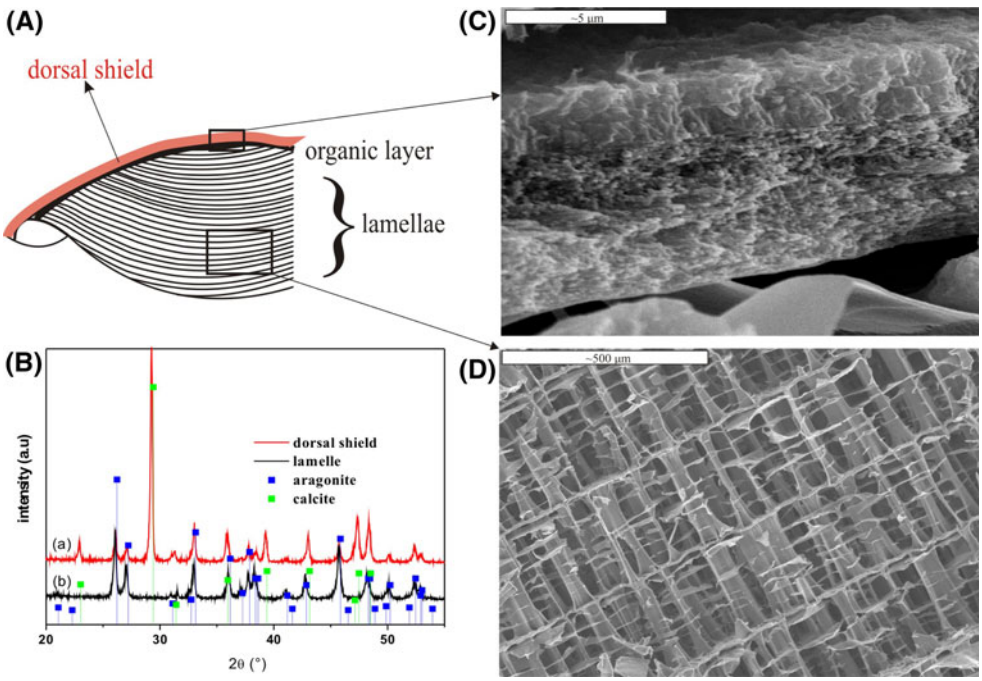

Fig. 1 **a** Schematic view of cross-section through the cuttlefish bone; **b** XRD patterns of the cuttlefish bone heat-treated at 350°C for 3 h, (*a*) dorsal shield, (*b*) lamellae spacing; **c**, **d** SEM micrographs of dorsal shield and lamellae spacing, respectively

Table 1 The change of phase composition and the pH values with HT treatment temperature

HT treatment temperature (°C)	Phases and pH of suspension after 20 min of HT treatment	
	pH[a]	Phases
140	5.34	Brushite, HA
160	5.45	Brushite, HA
180	5.75	HA
200	6.27	HA
220	6.42	HA

[a] Measured at room temperature

standard. XRD patterns clearly show that at the beginning of HT treatment, aragonite transforms rapidly to HA and 24 h HT treatment at 200°C was needed for complete transformation of aragonite into HA. In the samples HT treated at 220°C for longer than 24 h along to hydroxyapatite, monetite ($CaHPO_4$) was also determined.

The Rietveld refinement approach [22] allowed us to follow quantitatively the formation of HA as a function of temperature and time of HT treatment. The structure of hydroxyapatite reported by Sundarsanan and Young [25] was used as a structural model in the Rietveld refinement. The scale factor, zero displacement, background coefficients, unit cell axes and profile function parameters were refined first. In the second step atomic positions and site occupancies were also refined, while the temperature displacements were kept fixed. The background was described by Chebishev polynomial of 6th order, and the diffraction profile was modeled by Thompson-Cox-Hastings pseudo-Voigt peak-shape function. The refinement of aragonite was performed mutually with HA and the structure was taken from the ICSD card No. 034308 [26]. For the silicon standard, only the scale factor and profile parameters were refined. Rietveld output of XRD data for the sample HT treated at 200°C for 24 h is given in Fig. 4 as an example. The changes of unit cell parameters of hydroxyapatite with time for samples HT treated at 180, 200 and 220°C are given in Table 2.

The unit cell parameters of HA formed at 180°C exhibited larger *a*-and *c*-axes than are those for HA in the samples treated at 200°C and larger than those in the literature [24] ($a = 9.432$ Å; $c = 6.881$ Å). With time of the HT treatment the parameters for all three temperatures decrease and approach to similar values: *a* varies between 9.4268 and 9.4289 Å, and $c = 6.89438$–6.8978 Å.

The quantity of converted HA as a function of the HT treatment time and temperature is shown in Fig. 5. As seen in the Fig. 5a, the sample HT treated at 180°C for 48 h contained 95.4 wt% of HA and 4.6 wt% of untransformed aragonite, while in the sample treated at 200°C for 24 h aragonite transformed completely into hydroxyapatite. On the other hand, the sample treated at 220°C for 24 h contained 97.9 wt% of HA, and 2.1 wt% of untransformed aragonite, while for longer treatment time (48 h), the amount of hydroxyapatite decreased on account of monetite, $CaHPO_4$, which was determined in quantity of 3.2 wt%. The results for the samples HT treated at 140 and 160°C are given in Fig. 5b. The largest fraction of HA in these samples after 48 h treatment is ~82 and ~94 wt%, respectively. In the sample HT treated at 160°C for 48 h small amount of calcite was also determined. The change of crystallite size was followed using Scherrer's approximation and Si standard to correct the instrumental broadening. As shown in Fig. 6, the crystallite size increases with the time of HT treatment faster along to the *c*-axis than along to *a*-axis. The maximum value is attained for the sample HT treated at 200°C for 48 h (about 75 nm).

3.2 FTIR spectroscopy

The FTIR spectra of HT treated samples are divided in two groups; the spectra of samples containing brushite as an intermediate crystalline form after HT treatment for 20 min (spectra at 140 and 160°C), and the spectra containing no brushite for the same duration time (spectra at 180, 200 and 220°C). From the first set of data, the spectra of the sample HT treated at 160°C for various times are given in Fig. 7. The spectrum of heat-treated cuttlefish bone at 350°C for 3 h is also attached. The spectrum of cuttlefish bone reveals the IR active CO_3^{2-} bands of aragonite at 1446 cm^{-1} (ν_3), 1082 cm^{-1} (ν_1), 852 cm^{-1} (ν_2), and doublet at 712 cm^{-1}, 710 cm^{-1} (ν_4) The formation of HA by HT treatment is evident according to characteristic bands of PO_4^{3-} tetrahedra: (ν_3 1042 and 1088 cm^{-1}; ν_4 602 and 563 cm^{-1}; ν_1 960 cm^{-1} and ν_2 470 cm^{-1}) [28]. The spectrum recorded after 20 min of HT treatment shows rather poorly resolved phosphate bands and the absence of characteristic stretching and bending vibrations of OH^- at 3570 and 630 cm^{-1}, respectively. With increase of HT treatment time, the intensities and resolutions of PO_4^{3-} bands are increased and OH^- band at 3570 cm^{-1} appears. The small intensity of OH^- bands is also characteristic for nanocrystalline biological apatites; probably because of a greater amount of carbonate ion incorporated in HA structure [29]. Accordingly, the same explanation could be valid for our results too. In general, there are two types of CO_3^{2-} substitutions in apatites; the substitution at the OH^- site

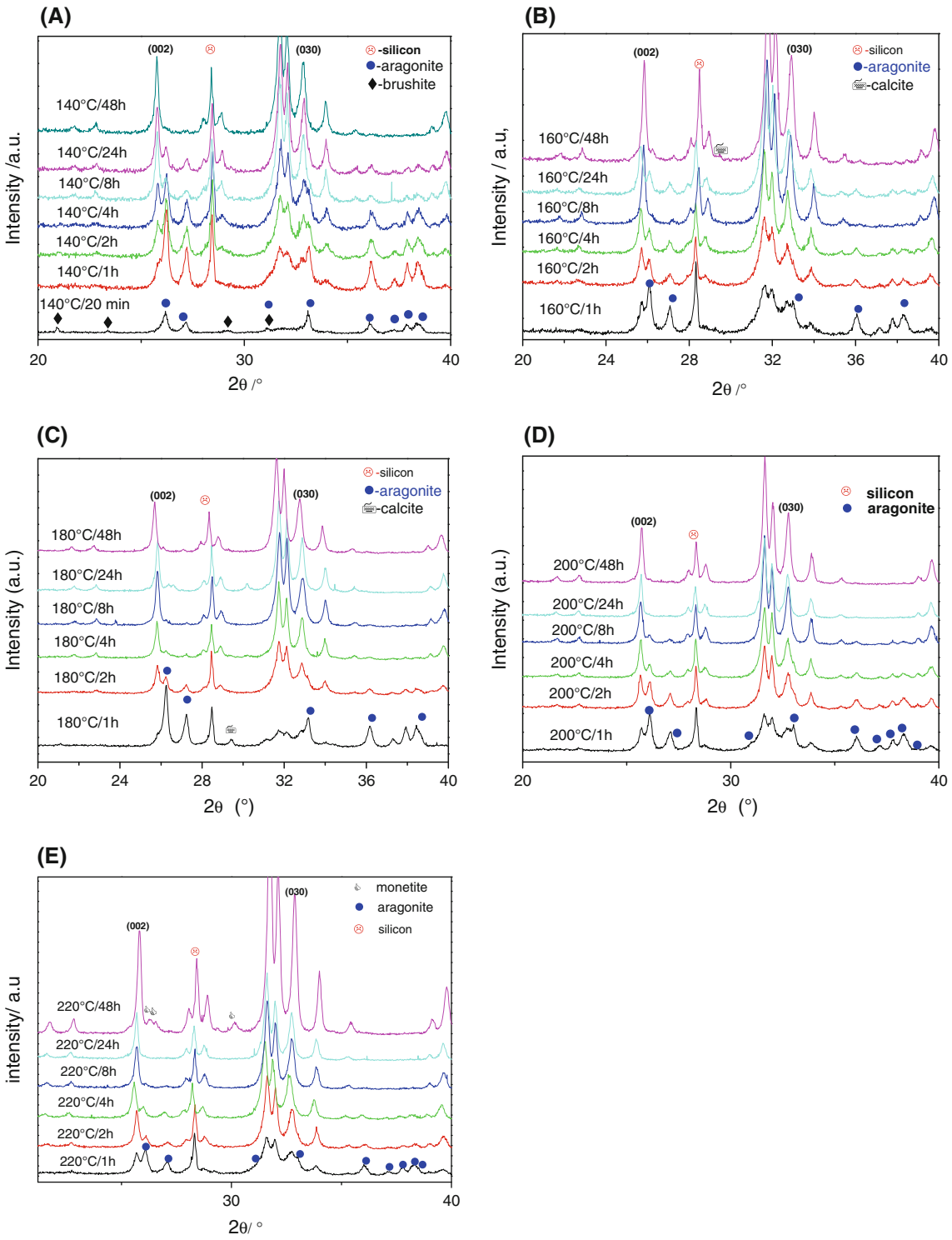

Fig. 3 XRD patterns of studies samples HT treated at: **a** 140°C; **b** 160°C; **c** 180°C; **d** 200°C and **e** 220°C

(A-type) and at the PO_4^{3-} site (B-type) [30, 31] which is reflected on the FTIR spectra. The broad bimodal peaks at 1412 and 1446 cm^{-1} and the peak at 872 cm^{-1} confirms carbonate ion in the B-site of HA structure. The bands not belonging to HA such as the shoulder at about 1110 cm^{-1} could be attributed to v_6 degenerated stretching of HPO_4^{2-} ions, which are usually found in brushite [32]. The existence of brushite in the samples HT treated at 140 and

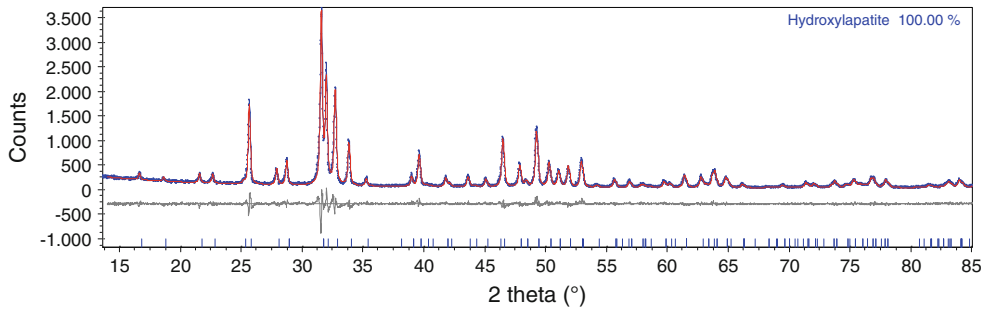

Fig. 4 Rietveld output of X-ray powder diffraction pattern of the sample heat-treated at 200°C for 24 h ($R_{exp} = 8.38$, $R_p = 9.34$, $R_{wp} = 12.03$). The *dots* are the experimental data, and the *solid line* the best-fit of profile. The difference between the experimental and fitted patterns is shown under the diffraction pattern. Line markers on the bottom of the figure indicate the position of Bragg reflections for hydroxyapatite

Table 2 Refined unit cell parameters of HA as a function of time and temperature

Time of treatment (h)	Hydrothermal treatment at 180°C			Hydrothermal treatment at 200°C			Hydrothermal treatment at 220°C		
	R_{wp}	a (Å)	c (Å)	R_{wp}	a (Å)	c (Å)	R_{wp}	a (Å)	c (Å)
1	0.109	9.4473(2)	6.878(2)	0.924	9.4441(3)	6.8930(4)	0.113	9.4454(3)	6.8945(3)
2	0.103	9.4427(3)	6.8995(3)	0.114	9.4352(4)	6.9017(3)	0.106	9.4362(3)	6.8988(3)
4	0.112	9.4361(1)	6.9044(1)	0.123	9.4368(3)	6.9017(3)	0.104	9.4298(3)	6.8984(3)
8	0.111	9.4356(3)	6.9024(1)	0.110	9.4244(3)	6.8987(2)	0.118	9.4306(4)	6.8973(3)
24	0.102	9.4359(2)	6.8984(2)	0.117	9.4251(3)	6.8902(2)	0.118	9.4252(3)	6.8902(3)
48	0.116	9.4289(2)	6.8978(2)	0.113	9.4281(2)	6.8938(2)	0.104	9.4268(2)	6.8938(2)

The R_{exp}, is the discrepancy factor that characterize a quality of the fit

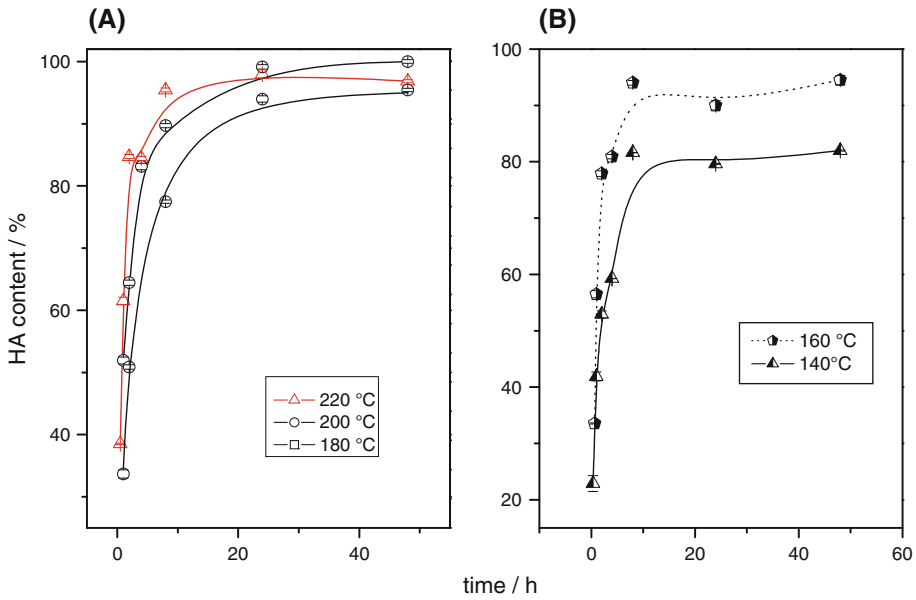

Fig. 5 Fraction of crystalline HA formed at various HT treatment time and temperature

160°C was also confirmed by XRD analysis as mentioned earlier (Fig. 2). When the cuttlefish bone is treated at 200°C, the OH^- stretching vibrations are visible already in the samples treated for 1 h and became more intense with duration of HT treatment, as shown in Fig. 8.

3.3 Crystallization kinetics

The isothermal kinetics of aragonite → hydroxyapatite transformation is described by the Johnson–Mehl–Avrami (JMA) equation [33, 34]

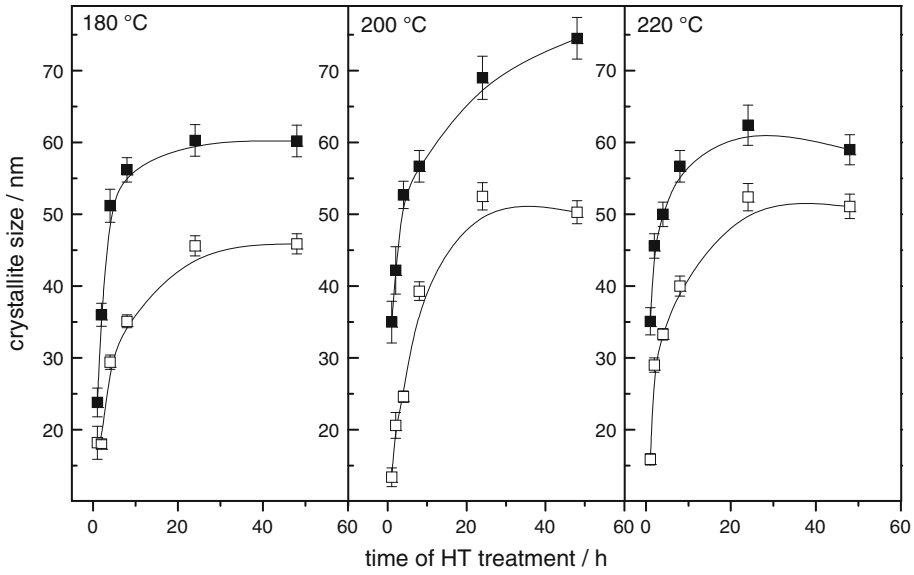

Fig. 6 Evolution of HA crystallite sizes; –■– along the $a = b$ axes and –□– c-axes, as a function of HT treatment temperature and time

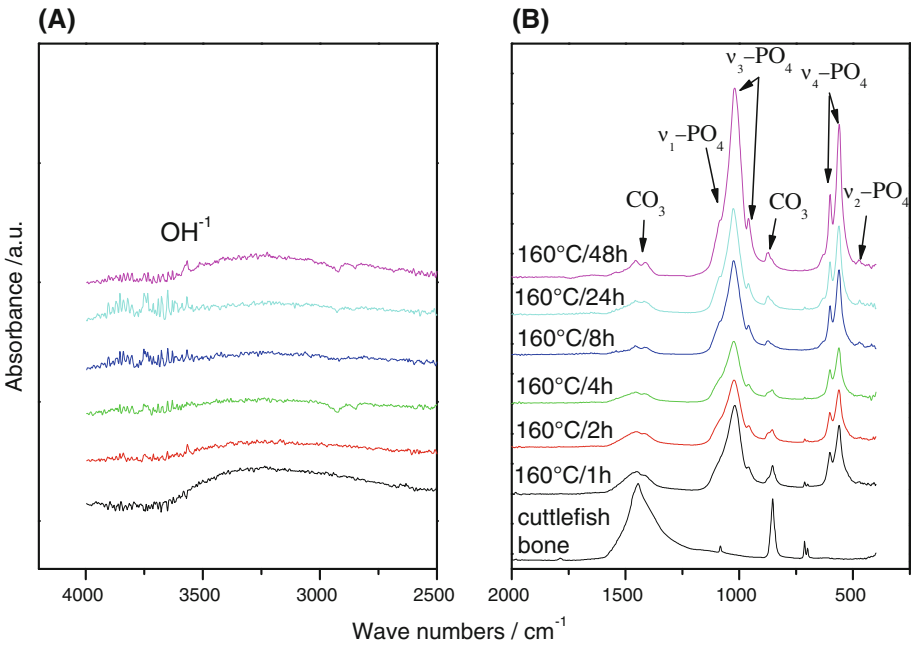

Fig. 7 FTIR spectra of hydrothermally converted HA at 160°C for various times: **a** FTIR spectra in the high energy region between 4000 and 2500 cm^{-1}; **b** FTIR spectrum of cuttlefish bone heated at 350°C for 3 h and converted spectra between 2000 and 450 cm^{-1}

$$\alpha = 1 - \exp[-(k^n(t-\tau)^n)], \quad (1)$$

where (α) is the fraction of transformed HA, n is the Avrami exponent, related to the nucleation type and growth dimension, τ is the incubation time, and k is the rate constant, which is the function of annealing temperature by assuming an Arrhenius relation:

$$k = k_0 \exp(-E_a/RT) \quad (2)$$

where k_0 is the frequency factor and E_a is the activation energy of crystallization. The fit of the Johnson–Mehl–Avrami model (Eq. 1) to the experimental data given in Fig. 5a and b are shown in Fig. 9, and the obtained constants n, k and τ are given in Table 3. Equation 1 can be written in double logaritmic form as $\ln(-\ln(1-\alpha)) = n \ln k + n \ln(t-\tau)$. This relationship indicates that a plot of $\ln(-\ln(1-\alpha))$ against $\ln t$ for different temperatures is expected to be linear. The value of n is then obtained from the slop of the best linear fitting of the experimental data. As shown in Fig. 10, the Avrami exponent remains constant and linear only in the time interval of $0 < t \leq 8$ h, however prolonged annealing (24 and 48 h) gives rise a significant deflection from the straight line. Taking into the consideration only the data between 1 and 8 h, the Avrami exponent ranges from 0.43 to 0.56 (Table 3). Allowing for experimental error, value of

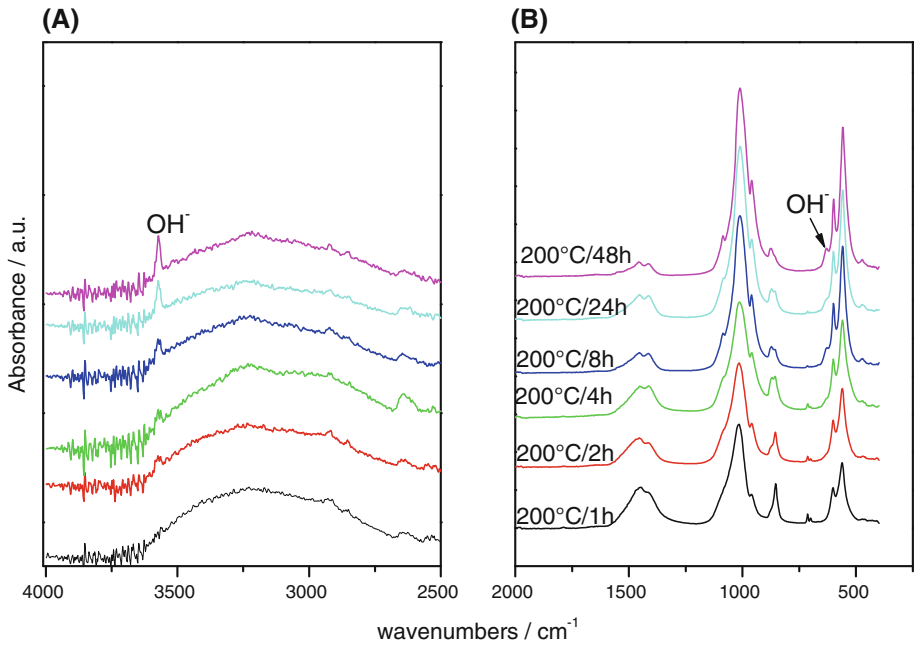

Fig. 8 FTIR of hydrothermally converted HA at 200°C for various times. **a** FTIR spectra in the high energy region between 4000 and 2500 cm^{-1}. **b** FTIR spectra between 2000 and 450 cm^{-1}. The assignment of bands is like in Fig. 7

(n) is close to $n = 0.5$. The activation energy of transformation can be determined by the slop of the plot ln k versus $1/T$, which is shown in Fig. 11. It. reveals the straight line only for temperatures 180, 200 and 220°C, and the activation energy of HA transformation is determined as $E_a = 77.8 \pm 5$ kJ/mol. The data for samples treated at 140 and 160°C show significant deflection from the linear plot, therefore, they were not taken into consideration for the Ea determination.

3.4 SEM observations of the HT treated samples

The microstructure of cuttlefish bones consists of two regions: a thick external wall or dorsal shield and internal regions with lamellae, which are separated by numerous pillars [35]. SEM micrographs in Fig. 12a and b show that the general image of cuttlefish bones was preserved after hydrothermal treatment and the cuttlefish bones retained its form with the same channel size (~80 × 300 μm). The enlarged view of transformed HA indicates the existence of many uniform, dandelion-like HA nanostructures with diameter from 3 to 8 μm, formed on the surface of lamellae and pillars (Fig. 13). With the prolonged HT treatment, the dandelion-like structures [36] are transformed into various nanostructure branches (Fig. 14a, b), which later form radially oriented nanoplates (Fig. 14c) and nanorods (Fig. 14d) with an average diameter of about 200–300 nm and an average length of about 8–10 μm.

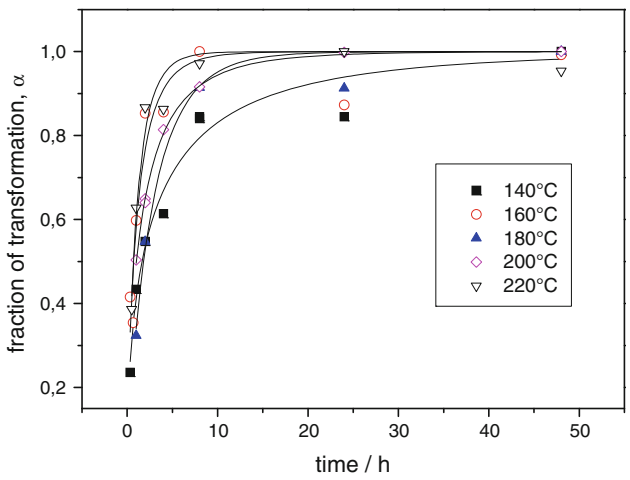

Fig. 9 The fit of the Johnson–Mehl–Avrami model (Eq. 1) to the experimental data given in Fig. 5a, b

4 Discussion

The reaction which takes place during the hydrothermal treatment of aragonitic cuttlefish bones with aqueous solution of ammonium dihydrogen phosphate could be described by the overall reaction (3).

$$CaCO_3 + NH_4H_2PO_4 + H_2O \rightarrow Ca_{10}(PO_4)_6(OH)_2 + 3(NH_4)_2CO_3 + 7H_2CO_3 \quad (3)$$

and the end product of the reaction is hydroxyapatite and evolved CO_2 and H_2O. Calcium carbonate is unstable under acidic pH values and introduced into ammonium dihydrogen phosphate solution partially dissolves and pH value of suspension increases from the starting value of pH 3.78 to various final values which depend on the time and temperature of treatment (For example, the suspension of

Table 3 Constants for the JMA relation $\alpha(t) = 1 - \exp(-(k^n(t-\tau)^n))$; $k = k_0\exp(-E_a/RT)$

Transformation	Temperature (°C)	k (h^{-1})	Avrami exp. n	Incubation time τ (h)	R^2
A → DCPD[a] & HA	HT 140°C	0.29 ± 0.05	0.56 ± 0.12	−0.212 ± 0.13	0.9769
A → DCPD[a] & HA	HT 160°C	1.6 ± 0.6	0.43 ± 0.11	0.58 ± 0.03 (34 min)	0.9824
A → HA	HT 180°C	0.32 ± 0.04	0.47 ± 0.04	0.57 ± 0.15 (32 min)	0.9985
A → HA	HT 200°C	0.697 ± 0.04	0.46 ± 0.09	0.408 ± 0.31 (24 min)	0.9919
A → HA & DCPA[b]	HT 220°C	1.7147 ± 0.9	0.43 ± 0.16	0.373 ± 0.16 (22 min)	0.9679

[a] The formation of well crystallized brushite (DCPD, $CaHPO_4{\cdot}2H_2O$) was determined in the samples treated for 20 min. These results were not considered for the evaluation of kinetics data

[b] Samples HT treated for 24 and 48 h contain monetite (DCPA, $CAHPO_4$)

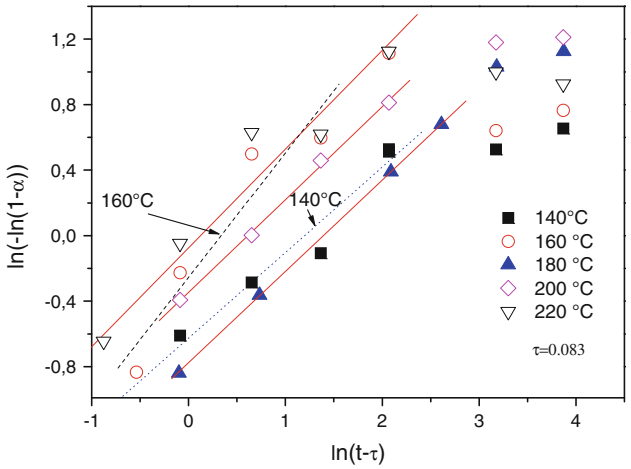

Fig. 10 The plot of $\ln(-\ln(1-\alpha))$ vs. $\ln(t-\tau)$ for different temperatures

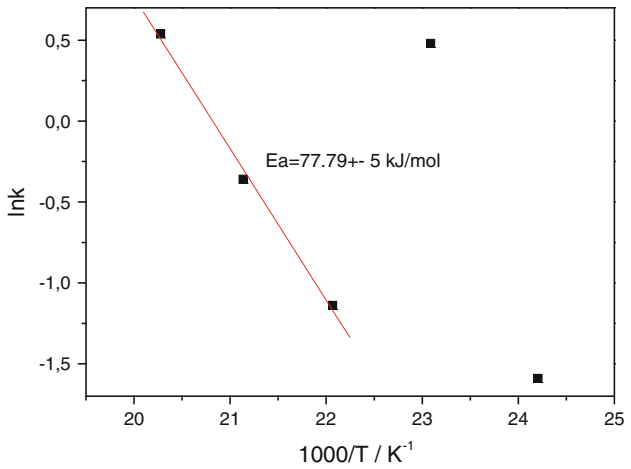

Fig. 11 The plot ln k vs. $1/T$

the sample HT treated at 200°C for 20 min yielded the pH 6.1 and for 1 h pH 7.0). As seen, the basic conditions in suspension is very soon attained and small amount of calcium ions, which were dissolved from the surface of aragonite reacted at the very near surface with phosphate ions, then precipitated as nuclei of HA and grew as HA crystals on the surface of aragonite. X-ray diffraction studies confirmed the formation of HA in samples HT treated at 180 and 200°C, and HA with a small amount of monetite for sample treated at 220°C for 48 h. On the other hand, $CaHPO_4{\cdot}2H_2O$, known as the mineral brushite, is a metastable compound which is normally observed as the primary crystalline product, when calcium phosphate is precipitated at low pH and low temperature [37]. According to pH values found in suspensions of samples treated at 140 and 160°C for 20 min (pH 5.34 and 5.45, respectively), the existence of brushite on XRD patterns treated for 20 min was understandable (Fig. 2). The shape of the (020) line of brushite indicates fairly well crystallized phase as the crystallization rate of brushite is much higher than that for HA [38]. Consequently, the existence of brushite in XRD patterns and HPO_4^{2-} band at about 1110 cm^{-1} on FTIR spectra for samples HT treated at 140 and 160°C (Fig. 7) are in accordance with literature [32]. The incorporation of CO_3^{2-} in the structure of HA is well documented with FTIR spectroscopy (Figs. 7 and 8). The absence of structurally bounded OH^- (or its presence in very small amounts) in the most CO_3^{2-} incorporated hydroxyapatite has been reported in a very recent work [37]. Therefore the incorporation of CO_3^{2-} in the structure of HA is correlated with the small intensities of stretching vibrations of OH^- in the high energy- and the middle energy-region. The unit cell parameters decrease with time of HT treatment, however, the decrease is not linear (Table 2), since the analyses were performed on bulk small pieces of natural cuttlefish bones. The non-uniformed changes of unit cell parameters with time (Table 2) are to be expected, since the samples are derived from natural sources. Crystallite size of HA also increases with time of HT treatment attaining the maximum values of ~60 nm for HT treatment at 180 and 220°C, and ~75 nm for HT treatment at 200°C. Rocha et al. [13] found that the crystallite size ranges from 20 to 50 nm. As seen in Fig. 5a only HT treatment at 200°C for 24 h gives rise to complete transformation of aragonite into HA, while at a lower temperature (180°C), aragonite was not yet completely

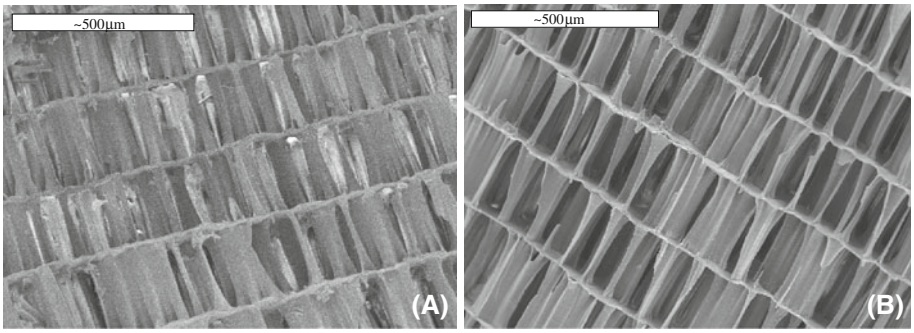

Fig. 12 Comparison of SEM micrographs of aragonite heat treated at 350°C for 3 h and the SEM micrographs of converted HA treated at 200°C for 24 h

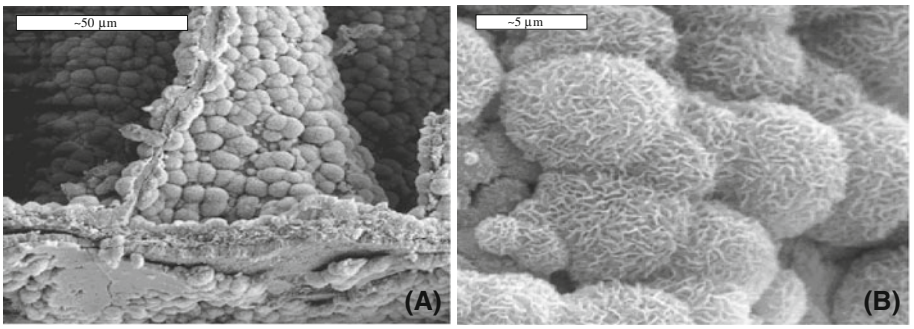

Fig. 13 SEM micrograph of the dandalion-like hydroxyapatite nanostructures

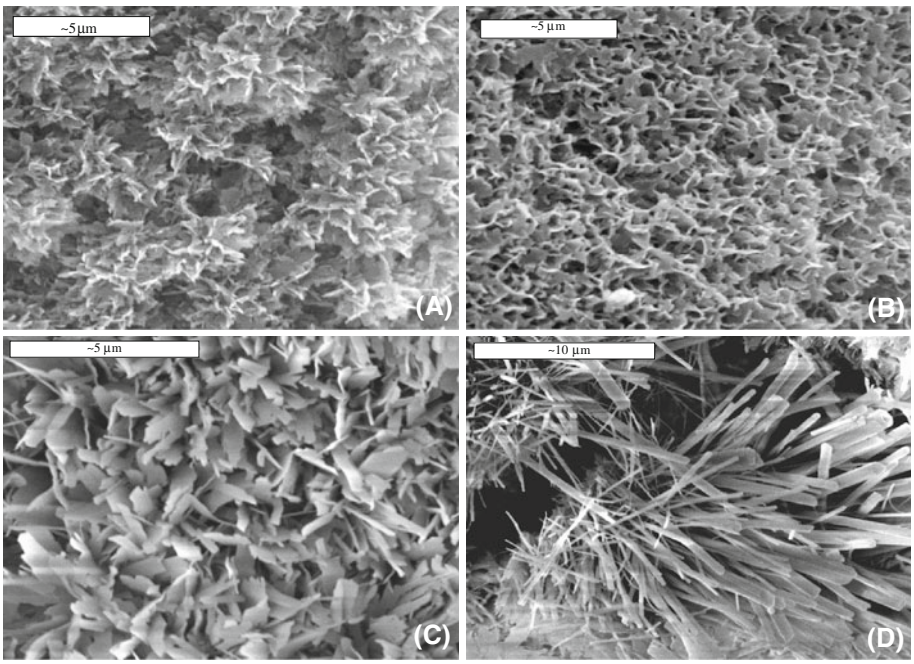

Fig. 14 SEM images of nanoplates and nanorods of HA

transformed even after 48 h of HT, and the fraction of transformed hydroxyapatite yields about 95%. On the contrary, higher HT treatment temperature (220°C) caused the formation of anhydrous calcium hydrogen phosphate, $CAHPO_4$ (monetite) above 4 h of HT treatment.

The results of kinetics analysis (Figs. 10, 11 and Table 3) show that the HT treatment temperature accelerated the formation of HA, and the rate constant, k, is increased with temperature, as expected for a thermally activated, or Arrhenius processes. However, the change of the rate constant with temperature is not uniform. Discrepancies are seen for the sample HT treated at 140°C, and especially for the sample treated at 160°C). It has to be emphasized, that XRD patterns of these samples treated for 20 min exhibited two crystalline phases; hydroxyapatite and metastable brushite. The latter phase disappears with duration time (Fig. 2). The kinetics of transformation is well described by JMA theory only when the rate constant

k remains constant all over the process [39]. However, in the samples HT treated at 140 and 160°C the mean rate constant of simultaneous crystallization of two phases (hydroxyapatite and brushite) is changing with time depending on the ratio of two phases. Accordingly, the required k constancy of the process is not fulfilled. On the other hand, almost the same Avrami exponent is obtained for all temperatures. The obtained value of Avrami exponent, n ($n \approx 0.5$) suggests that the growth mechanism of HA can be described as one dimensional growth of HA controlled by diffusion process for the whole temperature interval studied. On the use of Avrami exponent to describe the mechanism of growth, it should be emphasized that this value depends on nature of both the nucleation and the growth processes. Accordingly, the definitive determination of growth mechanism requires independent determination of one of these processes [40]. The anisotropic growth of HA along the a-axis (Fig. 6) and changes of the morphology of HA structures from 3D dandelion-like HA assemblies to the radially oriented nanoplates (Fig. 14c) and nanorods (Fig. 14d) of HA suggest that the above mechanism of HA growth could be operative. The change in morphology with the time of HT treatment thus reflects this difference in growth rates. The metastable phase (brushite) that appeared at the early stage of transformation (140 and 160°C), with the increasing reaction temperature or the time will transform to thermodynamically stable phase of HA. These results are consistent with those reported in the literature [41]. Comparing with the reaction time, the temperature of reaction is more significant variable in changing the morphology of HA.

5 Conclusion

- Transformation of aragonitic cuttlefish bones into hydroxyapatite using hydrothermal treatment at temperatures between 140 and 220°C for various times (1–48 h) has been investigated. In the initial reaction step at 140 and 160°C small amount of brushite ($CaHPO_4 \cdot 2H_2O$) was crystallized, due to acidic conditions of the suspension in the pressure vessel. In extended times conditions ($t > 1$ h) aragonite converted completely into HA.
- The kinetics and mechanism of transformation was studied using results of quantitative XRD analysis and Rietveld structure refinement. The Avrami formalism was used to describe the rate of crystallization, and the kinetics data were evaluated on the hydrothermally treated samples at 180, 200 and 220°C. HT treatment temperature accelerated the formation of HA, and the rate constant, k, increased with temperature, as expected for thermally activated process. The activation energy of transformation equals $E_a = 78 \pm 5$ kJ/mol.
- The interconnecting porous morphology of the starting material (aragonite) was maintained during the HT treatment. With extended time, HA was anisotropically grown along the a-axis and the dandelion-like HA nanostructures were formed.
- Based on the results of kinetics data and on the microstructural observation, the crystallization of HA is best determined by one dimensional growth controlled by diffusion.
- 3D structures using the natural morphology of cuttlefish bones offer promising alternatives for bone tissue engineering application.

Acknowledgments The financial support of the Ministry of Science, Education and Sports of the Republic of Croatia in the framework of the project "Bioceramic, Polymer and Composite Nanostructured Materials" (No.125-1252970-3005) and Universidad Politecnica de Valencia (Centro de Biomateriales), Spain is gratefully acknowledged.

References

1. Hench LL, Wilson J. Introduction to bioceramics. Singapore: World Scientific; 1993.
2. LeGeros RZ, LeGeros JP. Dense hydroxyapatite. In: Hench LL, Wilson J, editors. Introduction to bioceramics. Singapore: World Scientific; 1993. p. 138–90.
3. Shin H, Jo S, Mikos AG. Biomimetic materials for tissue engineering. Biomaterials. 2003;24:4353–64.
4. Wilson CE, de Bruijn JD, van Blitterswijk CA, Verbout AJ, Dhert WJA. Design and fabrication of standarized hydroxyapatite scaffold with a defined macro-architecture by rapid prototyping for bone-tissue engineering research. J Biomed Mater Res A. 2003;68A:123–32.
5. Lemos AF, Ferreira JMF. Designing of bioceramics with bone-like structures tailored for different orthopedic applications. Key Eng Mater. 2004;254–256:1037–40.
6. LeGeros LZ. In: Brown PW, Constantz B, editors. Hydroxyapatite and related materials. Boca Raton: CRC Press; 1994.
7. Murugan R, Ramakrishna S, Rao KP. Nanoporous hydroxy-carbonate apatite scaffold made of naturale bone. Mater Lett. 2006;60:2844–7.
8. Murugan R, Ramakrishna S. Production of ultra-fine bioresorable carbonated hydroxyapatite. Acta Biomater. 2006;2:201–6.
9. Hu J, Russell JJ, Ben-Nissan B, Vago R. Production and analysis of hydroxyapatite from Australian corals via hydrothermal process. J Mater Sci Lett. 2001;20:85–7.
10. Vecchio KS, Zhang X, Massie JB, Wang M, Kim CW. Conversion of bulk seashells to biocompatible hydroxyapatite for bone implants. Acta Biomater. 2007;3:910–9.
11. Ni M, Ratner BD. Nacre surface transformation to hydroxyapatite in a phosphate buffer solution. Biomaterials. 2003;24:4323–31.
12. Rocha JHG, Lemos AF, Agathopoulos S, Valério P, Kannan S, Oktar FN, Ferreira JMF. Scaffolds for bone restoration from cuttlefish. Bone. 2005;37:850–7.
13. Rocha JHG, Lemos AF, Kannan S, Agatholopoulos S, Ferreira JMF. Hydroxyapatite scaffolds hydrothermally grown from aragonitic cuttlefish bones. J Mater Chem. 2005;15:5007–11.

14. Rocha JHG, Lemos AF, Agatholopoulos S, Kannan S, Valerio P, Ferreira JMF. Hydrothermal growth of hydroxyapatite scaffolds from aragonitic cuttlefish bones. Biomed Mater Res A. 2006; 77A:160–8.
15. Eysel W, Roy DM. Topotactic reaction of aragonite to hydroxyapatite. Z Kristallogr. 1975;141:11–24.
16. Zaremba CM, Morse DE, Mann S, Hansma PK, Stucky GD. Aragonite-hydroxyapatite conversion in gastropod (abalone) nacre. Chem Mater. 1998;10:3813–24.
17. Yoshimura M, Sujaridworakun P, Koh F, Fujiwara F, Pongkau D, Ahniyaz A. Hydrothermal conversion of calcite crystals to hydroxyapatite. Mater Sci Eng C. 2004;24:521–4.
18. Jinawath S, Polchai D, Yoshimura M. Low-twemperature hydrothermal transformation of aragonite to hydroxyapatite. Mater Sci Eng C. 2002;22:35–9.
19. Huang LY, Xu KW, Lu J. A study of the process and kinetics of electrochemical deposition and the hydrothermal synthesis of hydroxyapatite coatings. J Mater Sci Mater Med. 2000;11: 667–73.
20. Liu CS, Huang Y, Shen W, Cui JH. Kinetics of hydroxyapatite precipitation at pH 10 to 11. Biomaterials. 2001;22:301–6.
21. Lopatin CM, Pizziconi VB, Alford TL. Crystallization kinetics of sol–gel derived hydroxyapatite thin films. J Mater Sci Mater Med. 2001;12:767–73.
22. Young RA. The Rietveld method. International Union of Crystallography. Monographs on crystalography, vol. 5. Oxford: Oxford Press; 1993.
23. The software TOPAS V 2.1 of Bruker advanced X-ray solution. Karlsruhe, Germany: Bruker AXS; 2003.
24. Kay MI, Young RA, Posner AS. Crystal structure of hydroxyapatite. Nature. 1984;204:1050–2.
25. Sundarsanan K, Young RA. Significant precision in crystal structural details: holly springs hydroxyapatite. Acta Crystallogr B. 1969;25:1534–43.
26. Dickens B, Bowen JS. ICDD:76-0606. J Res Natl Bul Stand A. 1971;75:27.
27. Cullity BD. Elements of X-ray diffraction. 2nd ed. Adison Wesley: Reading, MA; 1978.
28. Lemos AF, Rocha JHG, Quaresma SSF, Kannan S, Oktar FN, Agatholopoulos S, Ferreira JMF. Hydroxyapatite nano-powders produced hydrothermally from nacreous material. J Eur Ceram Soc. 2006;26:3639–46.
29. Pasteris JD, Wopenka B, Freeman JJ, Rogers K, Valsami-Jones E, van der Houwen JAM, Silva MJ. Lack of OH in nanocrystalline apatite as a foncion of degree of atomic order: implications for bone and biomaterials. Biomaterials. 2004;25:229–38.
30. El Feki H, Savariault JM, Ben Salah A. Structure refinements by the Rietveld method of partially substituted hydroxyapatite: $Ca_9Na_{0.5}(PO_4)_{4.5}(CO_3)_{1.5}(OH)_2$. J Alloys Compd. 1999;287: 114–20.
31. Landi E, Celotti G, Logroscino G, Tampieri A. Carbonated hydroxyapatite as bone substitute. J Eur Ceram Soc. 2003;23: 2931–7.
32. Hong ZD, Luan L, Paik SB, Deng B, Ellis DE, Ketterson JB, Mello A, Eon JG, Terra J, Rossi A. Crystalline hydroxyapatite thin films produced at room temperature an opposing radio frequency magnetron sputtering approach. Thin Solid Films. 2007;515:6773–80.
33. Johnson WA, Mehl RF. Reaction kinetics in procesess of nucleation and growth. Trans Am Inst Min Eng. 1939;135: 416–42.
34. Avrami M. Kinetics of phase change. J Chem Phys. 1941;9:177–84.
35. Birchall JD, Thomas NL. On the architecture and function of cuttlefish bone. J Mater Sci. 1983;18:2081–6.
36. Liu JB, Li KW, Wang H, Zhu M, Yan H. Rapid formation of hydroxyapatite nanostructures by microwave irradiation. Chem Phys Lett. 2004;396:429–32.
37. Lundager Madsen HE. Influence of foreign metal ions on crystal growth and morphology of brushite ($CaHPO_4{\cdot}2H_2O$) and its transformation to octacalcium phosphate and apatite. J. Cryst Growth. 2008;310:2602–12.
38. Oliveira C, Ferreira A, Rocha F. Dicalcium phosphate dihydrate precipitation. Characterization and crystal growth. Chem Eng Res Des. 2007;85:1655–61.
39. Pérez-Maqueda LA, Criado JM, Malek J. Combined analysis for crystallization kinetics of non-crystalline solids. J Non-Cryst Sol. 2003;320:84–91.
40. Christian JW. The theory of transformation in metals and alloys. 3rd ed. Oxford: Pergamon; 2002.
41. Tas AC, Bhaduri SB. Chemical processing of $CaHPO{\cdot}2H_2O$: its conversion to hydroxyapatite. J Am Ceram Soc. 2004;87:2195–200.